Thermal analysis of the tile impacted by concentrated heat loads caused by the loss of an upstream tile

Nomenclature

Pr – Prandtl number
Nu – Nusselt number
Re – Reynolds number
v_{ev} – evaporation rate
α – heat transfer coefficient
d – cooling channel diameter
b – area of lateral loading
s - tile width
h-heigt
L_{ev} – latent heat of evaporation
x – coordinate
y - coordinate
Y-tape twist ratio
q – heat flux
t - temperature
λ - heat conductivity
P - pressure
w – water velocity
M – molecular mass
k_a – accommodation coefficient
F_{xy-N} – form factor
c - heat capacity
ν - kinematic viscosity
ρ - density

indexes:

load –heat from plasma
w – wall
b – water
cr – critical
n - normal
eff - effective
sat - saturation

Introduction

Together with the technical and functional requirements imposed on the divertor target developed for the ITER-FEAT machine, there is a goal for the cost of the ITER-FEAT divertor to be 50 % of the 1998 ITER design value [1]. A selection of a flat tile design for the lower part of vertical target as a less expensive than the reference CFC monoblock design could be complied with the main design drivers – to reduce the cost as possible. However, due to concerns over the observed tendency for flat CFC tiles to suddenly and totally detach, this option is considered as a back-up to the reference monoblock. Actually, loss of a single tile itself might be tolerated and does not drive mandatory to departure from the machine normal operation. What is not acceptable is a possible cascade failure, when loss of a single tile causes the heat load to the next tile to be doubled, which can lead to its detach for some reasons and so on. That is why, it was extremely important to investigate this phenomenon, i. e. process, which can be triggered by a single tile failure.

Only a thermal-physical aspect of this problem has been under consideration, i. e.

- tile evaporation resulting in the loaded surface erosion (part of surface material is brushed out);
- redistribution of the temperature field and heat fluxes inside the armour and heat sink due to highly concentrated lateral heat load and surface burn-out;
- shifting of the heat removal mode closer to CHF.

Besides the above-mentioned points of interest, the obtained results of the thermal analysis (temperature and heat flux distribution near tile/heat sink joints) might be applied further for the mechanical analysis of the consequences caused by the tile failure.

1. Objectives

To resolve the problem discussed above, first of all, it was necessary to develop a new code (2-D at least) with ability to simulate the evolution in time of the surface profile due to its expected erosion, because the available and widely used for thermal and stress analysis codes, such as ANSYS, COSMOS, ABACUS, are not able to do that.

As a such, the following objectives were formulated for the performed study:

- to develop the mathematical model, which allows us to simulate all peculiarities of the process being under consideration;
- basing on the thermal analysis performed by the developed code to investigate possible consequences of a flat tile failure with the ultimate goal to define the design options and operational parameters window make possible to avoid the cascade effect during transients.

2. 2-D code development and verification

An experience on the development of codes for simulation of the high heat flux and the solid surface interactions (simulation of plasma-surface interaction at plasma disruption in tokamaks [2,3,4,5], evaluation of heat transfer in multilayer targets, impacted by the high power electron beams [6]) was applied by authors for the development of the new code. The problem is only one of the developed previously codes were 1-D codes and, therefore, they could not be used directly in our study. The complexities of the problem lays in description and, mostly, in realization in 2-D Finite Element model the laws of the loaded surface motion due to its erosion. Finally, the optimal for the considered design options, materials and the load conditions method has been selected, which simulates the evolution of the surface profile due to the erosion by *the displacement of the mesh nodes according to the given laws (the mesh compression method).*

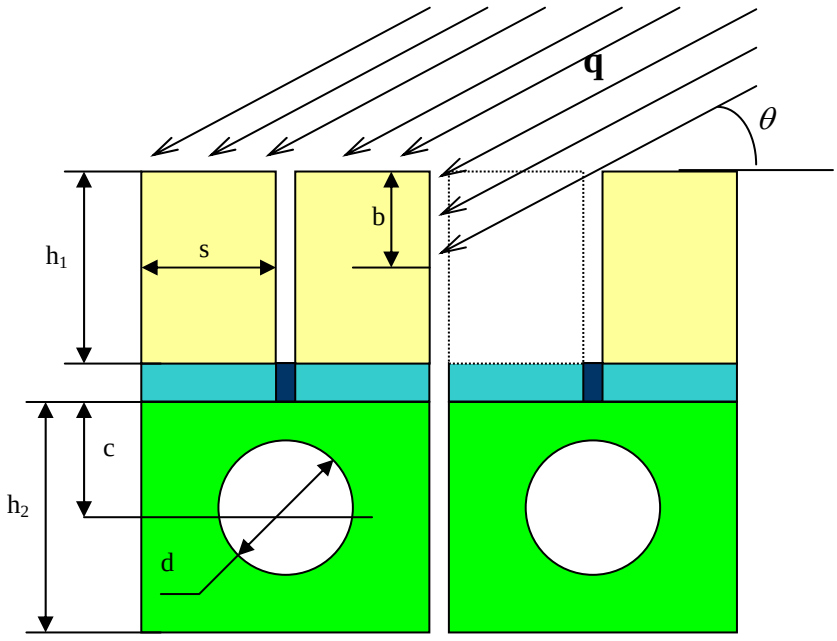

Fig. 1. 2-D model of Vertical Target for thermal analysis at one of the tile failure

So, summarizing the above mentioned, the following equation, described the 2-D transient non-linear temperature distribution in the 2-D solid body with the changeable loaded surface is put for the analysis:

$$c\rho\frac{\partial T(x,y)}{\partial \tau}=\frac{\partial}{\partial x}\left(\lambda_x\frac{\partial T(x,y)}{\partial x}\right)+\frac{\partial}{\partial y}\left(\lambda_y\frac{\partial T(x,y)}{\partial y}\right) \qquad (2.1)$$

The boundary conditions on the plasma facing surface (external boundary) of the vertical target might be written as (see Fig. 1):

$$-\lambda_n \frac{\partial T(x,y)}{\partial n}\Bigg|_{x,y\in S} = q_{load}(x,y) - q_{rad}(x,y) - \rho L_{ev}\frac{d\vec{S}(x,y)}{d\tau}\cdot\vec{n}(x,y) \qquad (2.2)$$

Here, the heat flux components on the target external surface are defined as follows:

$q_{load}(x,y) = \vec{q}_0 \cdot \vec{n}(x,y)$ - heat load from the plasma;

where: $|\vec{q}_0|$ = 382 MW/m^2 – heat flux at the plasma transients;

$\vec{n}(x,y)$ - the normal to the target outer surface;

$q_{rad}(x,y) = \sigma\varepsilon_{eff}F_{xy-N}(T^4(x,y) - T_{N0}^4)$ - heat lost by radiation on to the neighbouring surface (T_{N0} = 773 K is assumed);

where: σ = 5.67·10^{-8} W/m^2/K^4 – Stefan-Boltzmann constant;

ε_{eff} - effective emissivity;

F_{xy-N} - form factor between VT surface (S), neighbouring tiles and FW;

$T(x,y)$ - surface temperature, K;

T_{N0} = 773 K temperature of surfaces enveloping the tile under analysis;

$\frac{d\vec{S}(x,y)}{d\tau} = -\nabla_{ev} = -\frac{k_a P_s}{\rho\sqrt{2\pi RT(x,y)/M}}\vec{n}(x,y)$, m/s – the velocity of moving of the tile loaded surface due to its evaporation (Knudsen-Lengmuir correlation for evaporation rates);

where: $\vec{S}(x,y)$ - tile external surface;

∇_{ev} - evaporation rate, m/s;

k_a -accommodation coefficient (taken k_a =1 for W and k_a =0.4 for CFC);

P_s - saturation pressure of the evaporated material, defined as a unction of the surface local temperature (see Fig.2);

ρ- tile material density, kg/m^3;

R = 8310 J/kmole/K- universal gas constant;

$T(x,y)$ - surface local temperature, K;

M – tile material molecular mass, kg/kmole;

L_{ev} = latent heat of evaporation, J/kg.

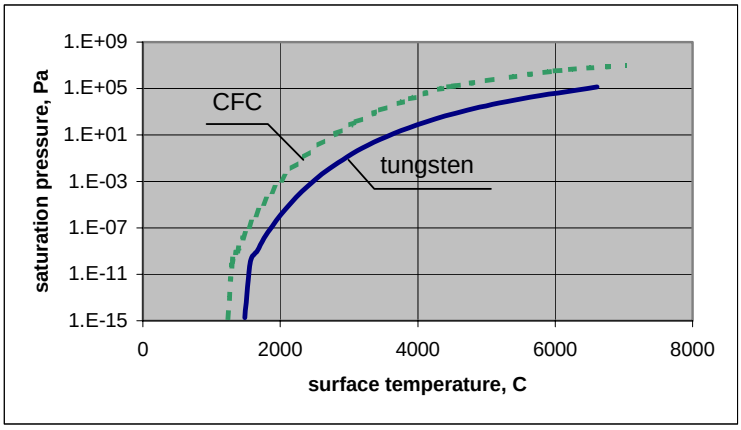

Fig. 2 Vapour saturation pressure for CFC & W

The boundary conditions on the channel inner surface cooled with water is described as:

$$-\lambda_n \frac{\partial T(x,y)}{\partial n}\Bigg|_{x,y\in S_1} = \alpha(T)(T(x,y) - T_{bulk}) \qquad (2.3)$$

where: $\vec{S}_1(x,y)$ - cooling channel inner wall;

$T(x,y)$ - local temperature of the wetted surface, °C;

T_{bulk} = 100°C – water bulk temperature (assumed to be a constant over process);

$\alpha(T)$ - local heat transfer coefficient as a function of the wetted wall temperature. This coefficient is determined from the boiling curve, which was build with accordance to the technique developed by the authors for the investigations of the heat exchange processes on the non-isothermal surface of the circular cooling channels with the twisted tape inserts under the subcooled water forced flow conditions. The boiling curve, similar to the depicted in Fig. 3, was used in the thermal hydraulic analysis of process related to the CHF problems [7,8].

So, in order to resolve the above stated problem (2.1) with the formulated boundary conditions (2.2-2..3) 2-D FE model with capability to simulate all the above discussed process peculiarities (evaporation, evolution of the loaded surface profile due to the loss of armour material, temperature depended heat transfer coefficient) has been developed (see Fig. 1). Some tests and application problems in 1-D approach have been solved to verify the developed code. The obtained numerical results were in a good agreement with the analytical solutions [9,10,11] as well as with the experiments [12]. All these results allow us to be confident in the code capability to provide the required analysis. However, more work is needed to verify the developed code comprehensively. This work is on our schedule and will be done as experimental data from the launched R&D tasks on study and tests of the cascade failure of flat tiles [1] become available.

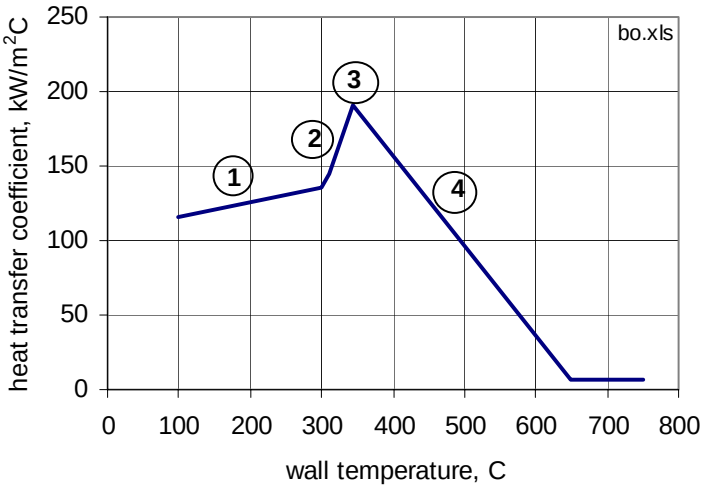

Fig. 3. Boiling curve for subcooled flow in a circular channel with the twisted tape as an enhancer.

P_{in} = 4.3 MPa, T_{bulk} = 100 C, w = 10 m/sec, Y = 2

1 – single phase convection mode: $Nu = 2.18 \cdot Y^{-0.09} \cdot 0.023 \cdot Re^{0.8} \cdot Pr^{0.4}$

2 – nuclear boiling mode: $T_{wall} - T_{sat} = 0.22 q^{0.357} exp(-P/8.6)$ – Thom' correlation

3 – CHF: $q\ CHF = c_f \cdot 0.23 \cdot f_0 \cdot G_{in} \cdot H_{fg} \cdot [1+0.00216 \cdot (P/22.1)^{1.8} \cdot Re_h^{0.5} \cdot Pr^{0.4}]$ – modified Tong-75

4 – post-CHF mode: empirical curve (results of treatment of numerical experiments on CHF)

3. Initial data and loading scenario

According to the task formulated by JCT the vertical target design options presented in Table 1. are taken for the thermal analysis. In addition to parameters shown in this Table, the following data are used too:

Heat sink material – CuCrZr;
Interlayer material – OFHC Cu;
Two design options for interlayer:

- interlayer separated for each tile by cutting (see Fig.1 – cutting down to heat sink, i.e. model w/o "black piece");
- common interlayer for all tiles (see Fig.1 – cutting to interlayer only, i.e. model with "black piece").

Cooling parameters:

-	water pressure,	p_{in}=4.3 MPa;
-	water temperature,	T_{bulk}=100°C;
-	water velocity,	w=10 m/s;
-	heat removal enhancer	twisted tape;
-	tape thickness	1 mm;
-	tape twist ratio,	Y=2.

Table 1. Geometric parameters of the tile design options being under analysis

Armour material	Symbol	W-alloys (1% La_2O_3)	CFC (MFC-1)	CFC (Dunlop)	Pure W*
Tile height, mm	h_1	5, 10	10, 15	10, 15	10
Tile width, mm	s	24.0, 11.75, 4.4	24.0, 11.75, 4.4	24.0	9.7
Heat-sink height, mm	h_2	20	20	20	20
Heat-sink width, mm	A	24	24	24	24
Interlayer thickness, mm		2	2	2	2
Gap between tiles, mm		0.5	0.5	0.5	0.6
Cooling channel diameter, mm	d	10, 14	10	10	12
Distance from interlayer to cooling channel axis, mm	c	8, 10	8	8	7
Area of lateral loading, mm	b	1.258, 0.655, 0.236	1.258, 0.655, 0.236	1.258	0
Angle between the tile surface and magnetic field line					

*Corresponded to mock-up tested in SNLA

Material thermo-physical properties for tungsten, tungsten alloy, CFC (MFC-1), CFC (Dunlop), CuCrZr, OFHC Cu are taken from "ITER PFC Materials Database".
As an example, two of them, namely, density and latent heat of evaporation for both materials W & CFC, one can find below:

$\overline{\rho}_{W}$ = 19200 kg/m^3 , L_{ev} = 4.96 10^6 J/kg for tungsten;

$\overline{\rho}_{CFC}$ = 1960 kg/m^3 , L_{ev} = 5.87 10^7 J/kg for CFC.

Heat loading scenario is shown in Fig. 4. Steady-state temperature distribution in the vertical target loaded by heat flux from the top only (q_n = 10 MW/m^2) is applied as an initial temperature state at the further transient analysis, when heat flux q_o = 382 MW/m^2 under a horizontal 3° angle impacts the tile next to the lost one within a single 10 seconds pulse.

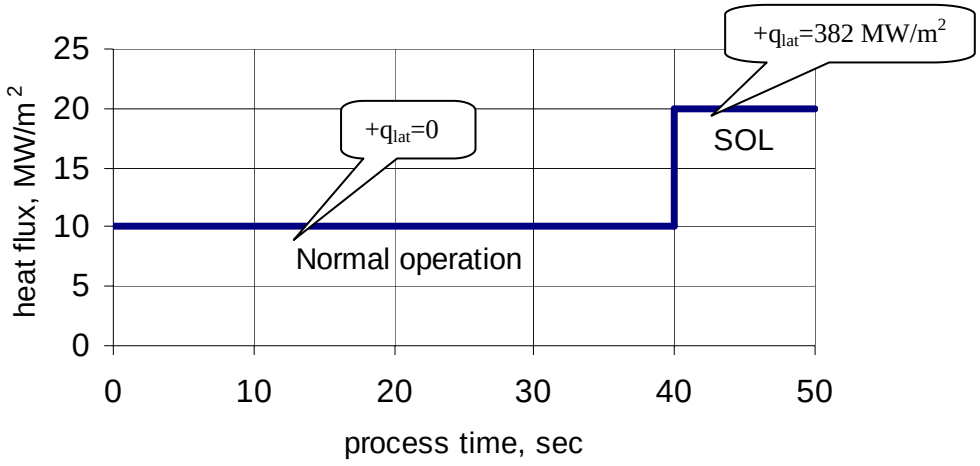

Fig. 4. Heat loading scenario

4. Results and discussions

The results of the thermal analysis of the tile intercepted the SOL by its leading edge at near normal incidence (flux q_o = 382 MW/m^2) due to the loss of an upstream tile are shown in the figures presented below.

The consequences of the lateral heat flux impact onto the receiving surface of the tungsten tile with the height (h_1) of 5 mm and with three tile widths (s) equal to 24 mm, 11.75 mm and 4.4 mm sequentially are demonstrated in Fig. 5.

In case of 24 mm tile, doubling of the integral heat load absorbed by water in the cooling channel results in the development of the heat removal global crisis, as it, strictly speaking, was expected, because the cooling system for the vertical targets has been designed with 1.4 safety margin only. It is therefore concluded, that the tungsten 24 mm width and 5 mm height tiles shall not be recommended as armours for the vertical target, because the lost of one of them, leads, certainly, to the development of the heat removal crisis in the cooling channel of the downstream tile subjected to the double integral load. This, in its turn, results in the burn-out of the cooling channel with water spilling into the Vacuum Vessel.

The evolution of the surface profile caused by the material erosion for the two tile width (s=11.7 mm and s=4.4 mm) are shown at the left side of Fig. 5 on the low graphs.

There are depicted, in sequence, at the right side of Fig.5:
- time history of the maximal erosion depth (displacement of the corner point A in horizontal direction) for the tile width: s=11.7 mm and s=4.4 mm;
- time history of the maximal surface temperature (in moving point A);
- evolution of the maximal heat flux absorbed by the tile surface.

The express analysis of the graphs presented in Fig.5 allows us to draw some useful conclusions.

First, the erosion of the tile surface results in the two consequences, at least: from one hand, in reduction of the heat load fraction transferred inside the tile body by conduction (see Fig.13&14) which facilitates the operational conditions of the armour/heat sink joints from the thermal stresses point of view, and from the other hand, to evolution of surface profile in such a manner that it results in the reduction of the maximum heat flux density as well as the maximum surface temperature. The surface temperature reduction brings to evaporation slow down and, finally, to its stopping.

Secondly, as it is seen from the graphs, though the erosion is slow down at the end of transients, but does not achieve its saturation condition within a single 10 seconds pulse. Our estimation shows, that for the stopping of the erosion process 3-10 pulses are required.

Thirdly, the tile width reduction from s=11.7 mm to s=4.4 mm results in the erosion decrease from 2.3 mm to 0.5 mm, but this erosion decrease, frankly speaking, is not a result of the tile width reduction itself, but it is a consequence of the reduction of the

area loaded by the lateral heat flux (b) in 2.5 times. If, due to any reasons (loss of two 4.4 mm neighbouring tiles in the same time, for example) the area loaded by lateral heat flux remains the same (b= idem), it seems, that the erosion depth dependence from the tile width, which we derived from graphs in Fig.5, does not valid in this case.

Fig. 6 shows the time history of the heat flux and the temperature distributions in the W/Cu joints (exactly on the boundary tile/interlayer) for 3 options of the tile width and for the design option with the separate interlayer for each tile. This design option we consider as a reference one. There are not graphs for 24 mm tile width in this figure, because they were not obtained due to the heat removal crisis, which took place in the cooling channel.

The analysis of the presented graphs shows, that the tile width reduction from s=11.7 mm to s=4.4 mm gives us the significant decrease of the maximum heat flux on the W/Cu boundary from 50 MW/m^2 to 38 –40 MW/ m^2 as well as the temperature drop along the boundary under a single tile from Δt = 400 C to δt = 30 ÷ 40 C, which makes possible to decrease significantly the thermal stresses in this region.

It should be stressed, that in case of 11.7 mm tile width the interlayer temperature exceeds its melting value over almost the half tile width. This fact needs to be analysed in details in order to foresee the possible consequences.

The similar graphs for the tungsten with the tile height (h_1) equals to 10 mm are shown in Fig.7 & 8.

One can see, that even though the tiles are not next to the lost one, the heat flux in their interlayer exceeds slightly the specified for the transients q_0=20 MW/m^2 (q_0~21 MW/m^2 and q_0~23 MW/m^2 for 11.7 mm and 4.4 mm tile width correspondingly, see Fig.6, 8, 10, 12). The reason is that gaps between the tiles (~0.5 mm) and 3° SOL incidence give us additional 1-3 MW/m^2 of heat loads for each the tile.

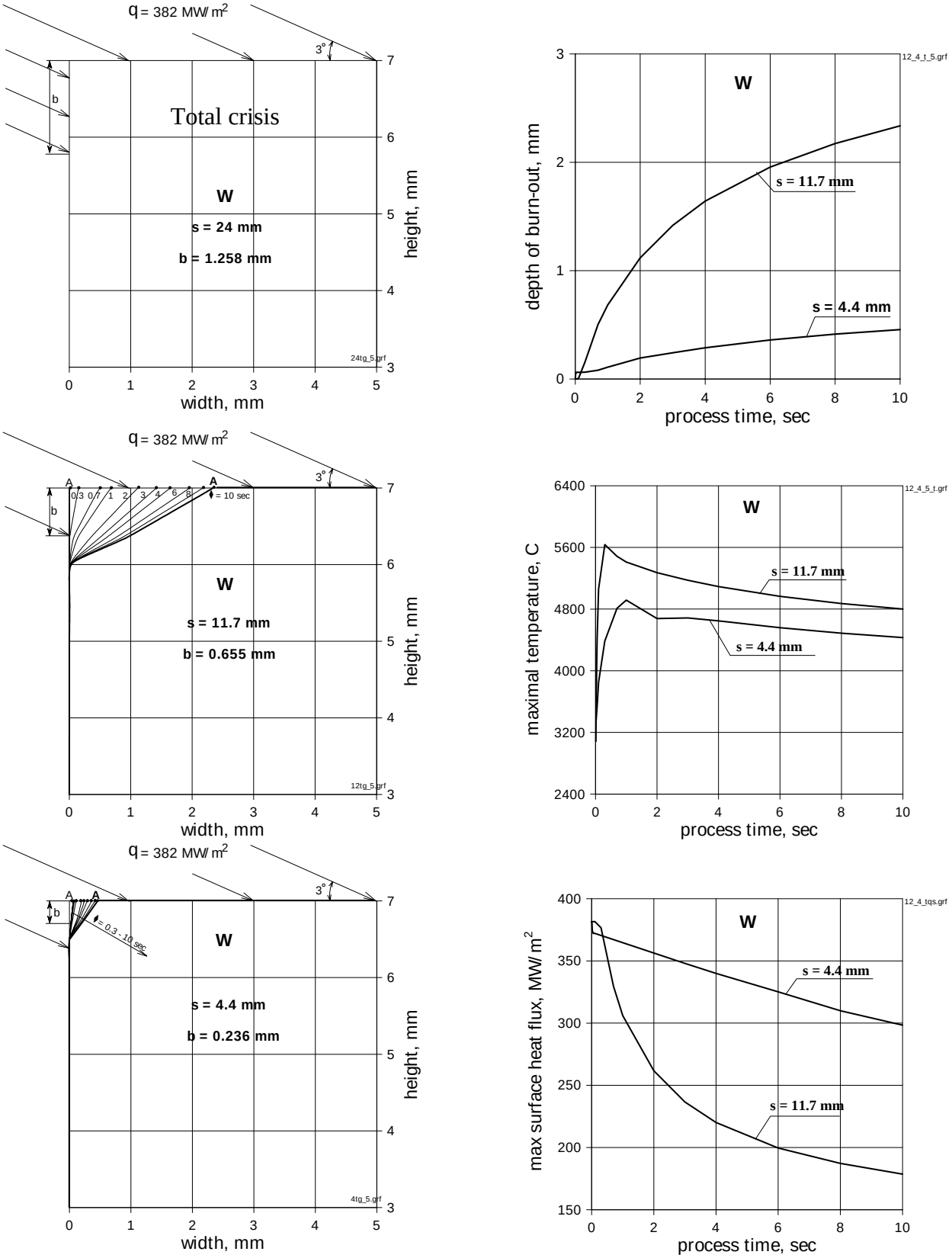

Fig. 5. Evolution of maximal temperature (A), maximal heat flux and surface profile at concentrated lateral heat load.

Material – W-alloy (1% La_2O_3), tile height (h_1) = 5 mm

Tile on separate interlayer

Tile width (s) = 4.4, 11.75, 24 mm

Area of lateral heat load (b) = 0.236, 0.655, 1.258 mm

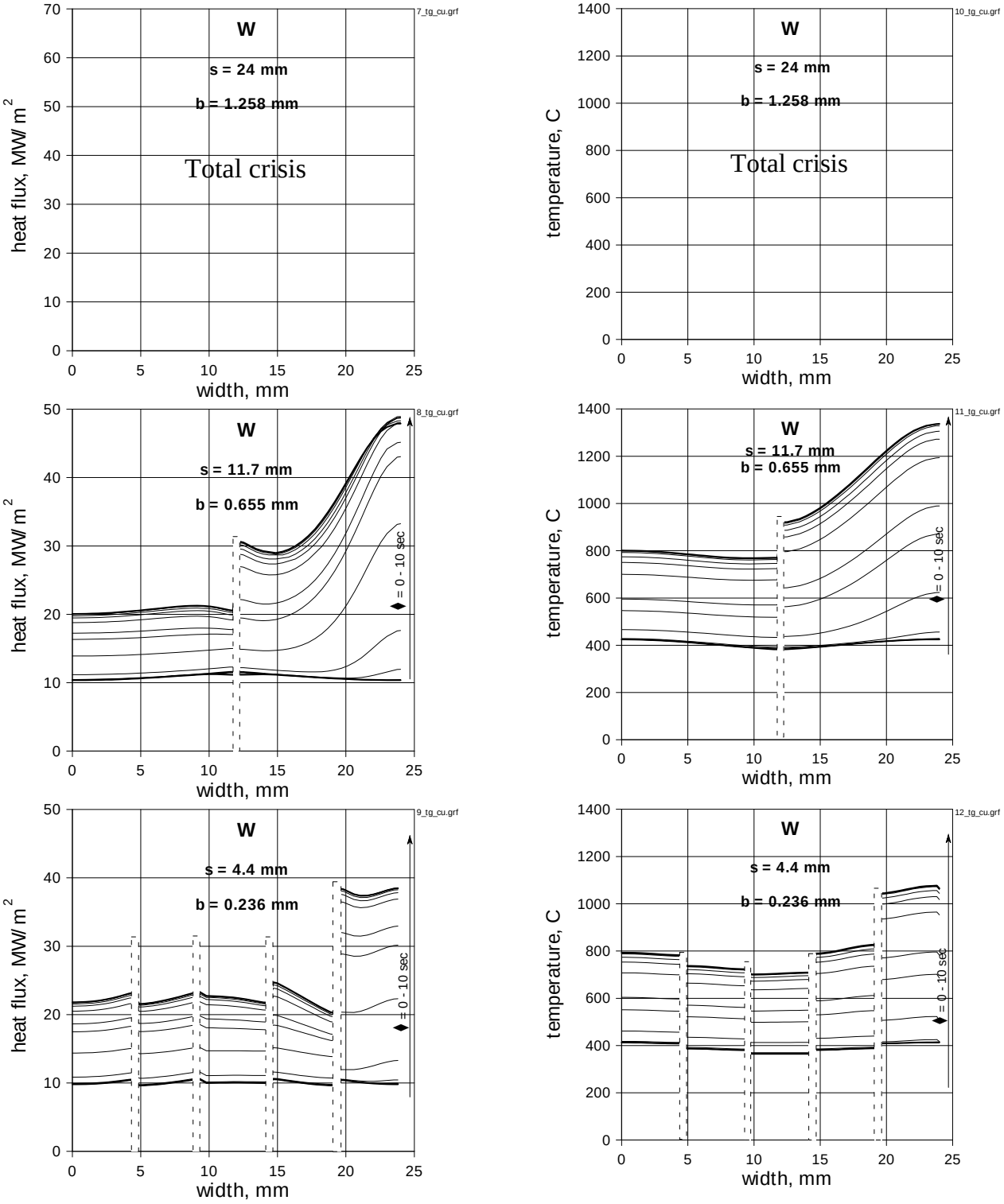

Fig. 6. Evolution of heat flux and temperature distribution in the W/Cu joint.

Material – W-alloy (1% La_2O_3), tile height (h_1) = 5 mm
Tile on separate interlayer
Tile width (s) = 4.4, 11.75, 24 mm
Area of lateral heat load (b) = 0.236, 0.655, 1.258 mm

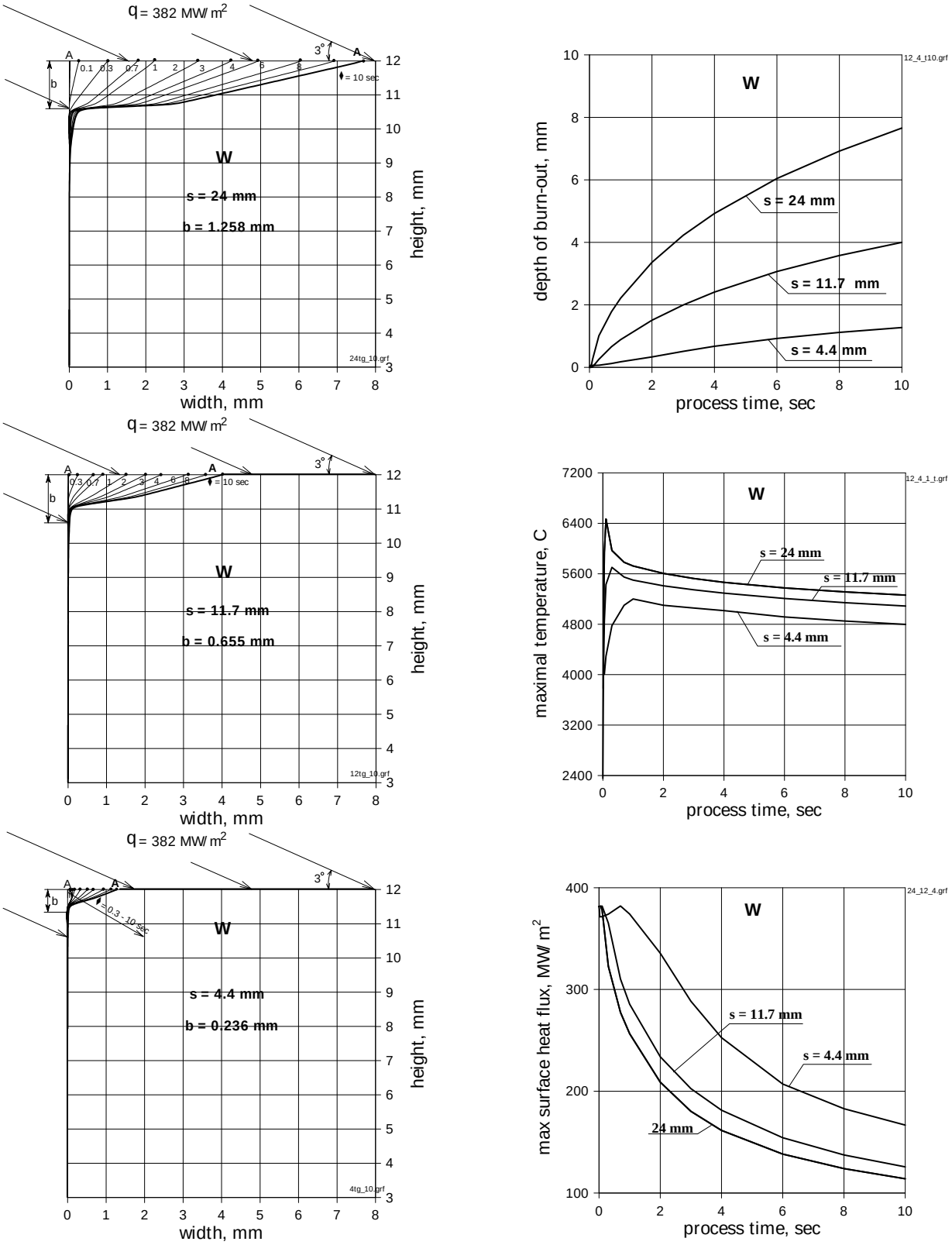

Fig. 7. Evolution of maximal temperature (A), maximal heat flux and surface profile at concentrated lateral heat load.

Material – W-alloy (1% La_2O_3), tile height (h_1) = 10 mm

Tile on separate interlayer

Tile width (s) = 4.4, 11.75, 24 mm

Area of lateral heat load (b) = 0.236, 0.655, 1.258 mm

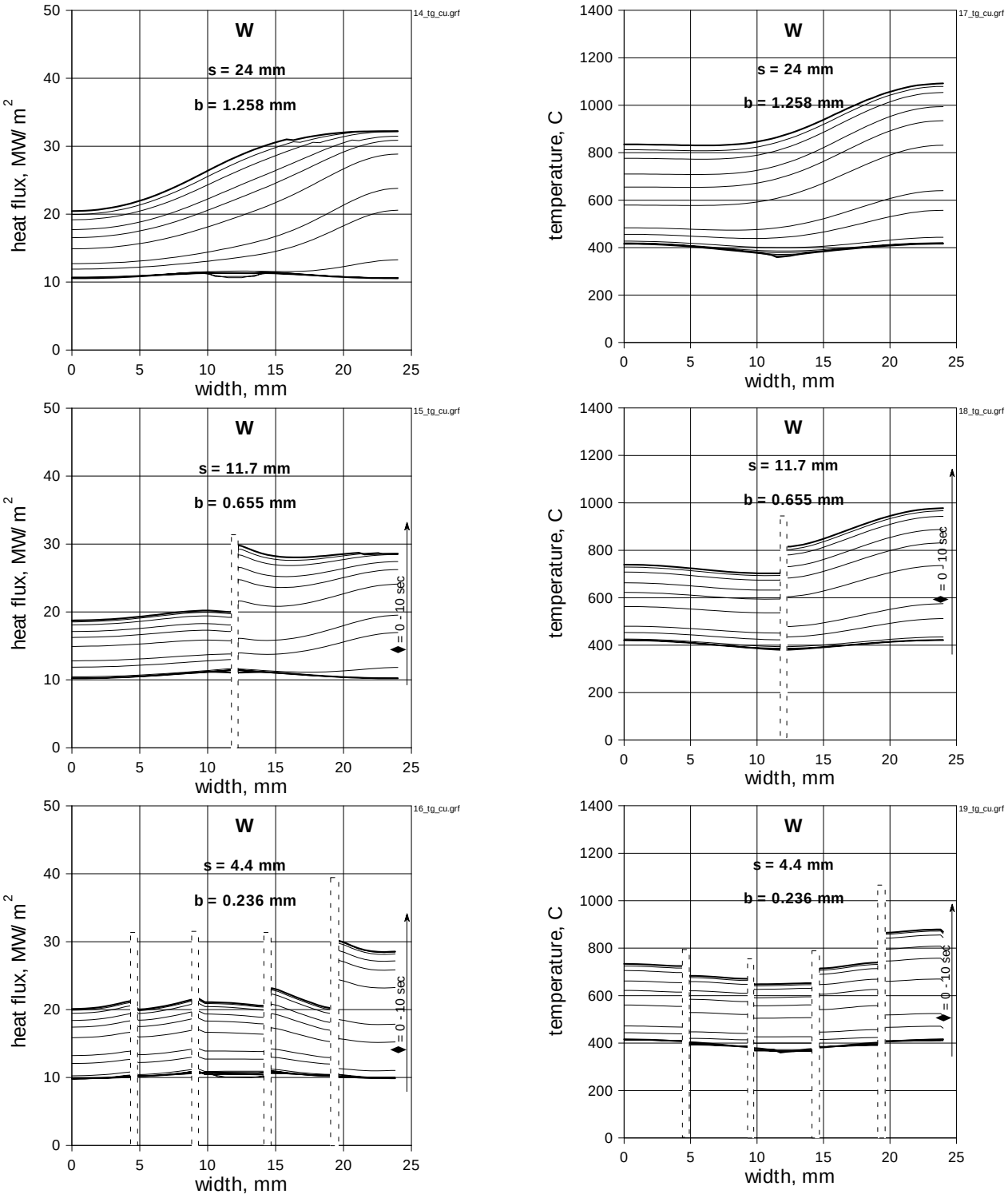

Fig. 8. Evolution of heat flux and temperature distribution in the W/Cu joint.

Material – W-alloy (1% La_2O_3), tile height (h_1) = 10 mm
Tile on separate interlayer
Tile width (s) = 4.4, 11.75, 24 mm
Area of lateral heat load (b) = 0.236, 0.655, 1.258 mm

It is seen clear, that the increase of the tile height in two times (from h_1=5 mm to h_1=10 mm) gives us the some changes in the obtained results.

First, unlike the previous results obtained for the short and wide tungsten tile (h_1=5 mm and s=24 mm), the stable solution takes place in this case for the wide tile (s=24 mm), i.e. the heat removal crisis is not observed here. It is happened, because the thermal resistance to heat transferred by conduction is increased due to the increase of the tile height in 2 times. As a result, the fraction of the heat lost by evaporation and radiation is increased as well. Latter leads to:

- the increase of the erosion depth from 2.4 mm to 4 mm and from 0.5 mm to 1 mm for the tile width 11.7 mm and 4.4 mm correspondingly;
- the reduction of the heat fraction transferred by the thermal conduction to the cooling channel, so the maximum heat flux in the interlayer is reduced from 50 MW/m^2 to 30 MW/m^2 and from 38 MW/m^2 to 30 MW/m^2 correspondingly;
- flattening of the heat flux distribution in the interlayer;
- the temperature reduction below the interlayer melting point for all three tile widths.

In case of the 10 mm tile height the fact, that the erosion process does not reach its saturation, is confirmed more clearly.

Next four figures (Fig. 9-12) demonstrate similar to the above process parameters obtained for 1-D graphite (CFC) with tile height (h_1) 10 mm and 15 mm subsequently.

Surprisingly, the erosion depth for both materials (W&CFC) does not much differ each from other (7.7 mm and 7.2 mm for W and CFC correspondingly), while their latent heats of evaporation differ significantly. This phenomenon is accounted for by their surface temperature difference (5600°C and 4000°C for W & CFC correspondingly), which equals the erosion depth.

Due to CFC 1-D conductivity the heat flux and temperature distribution in the joint area more non-uniform than it takes place in tungsten. That is why, to obtain the acceptable parameters on the CFC/Cu boundary the higher tile is a preferable. The results of computation presented in Fig. 11-12 for the tile height (h_1) equal to 15 mm confirm this conclusion.

As it shown in Fig. 15, the 3-D CFC (Dunlop) helps us to reduce slightly the heat flux non-uniformity in the joint region as well as a level of the maximum heat flux and temperature, but it gives us not much credit, especially, in case of high (15 mm) and thin (4.4 and 11.7 mm) tiles.

Fig. 13 and 14 show evolution of heat balance in time of transients. It is seen, that almost 20 % of the total heat load lost by radiation and due to evaporation. A contribution of the material evaporation in the heat balance is most considerable at the beginning of the transients (see Fig. 14).

An attempt has been made to decrease the temperature in the W/Cu joint below its melting point by two ways: (1) by increasing of the cooling channel diameter (d) from 10 mm to 14 mm and (2) by reduction of the thermal resistance between the interlayer and cooling channel. The graphs depicted in Fig. 16 demonstrate results of these

attempts. An increase of a cooling channel diameter gives us, practically, nothing, and only the reduction of copper ligament above the cooling channel (from 3 mm to 1 mm) makes it possible to decrease the interlayer temperature by 200°C (but it still remains above copper melting temperature for the tile height of 5 mm). But in this case (ligament thickness of 1 mm) reliability of heat sink should be confirmed by additional structural analyses.

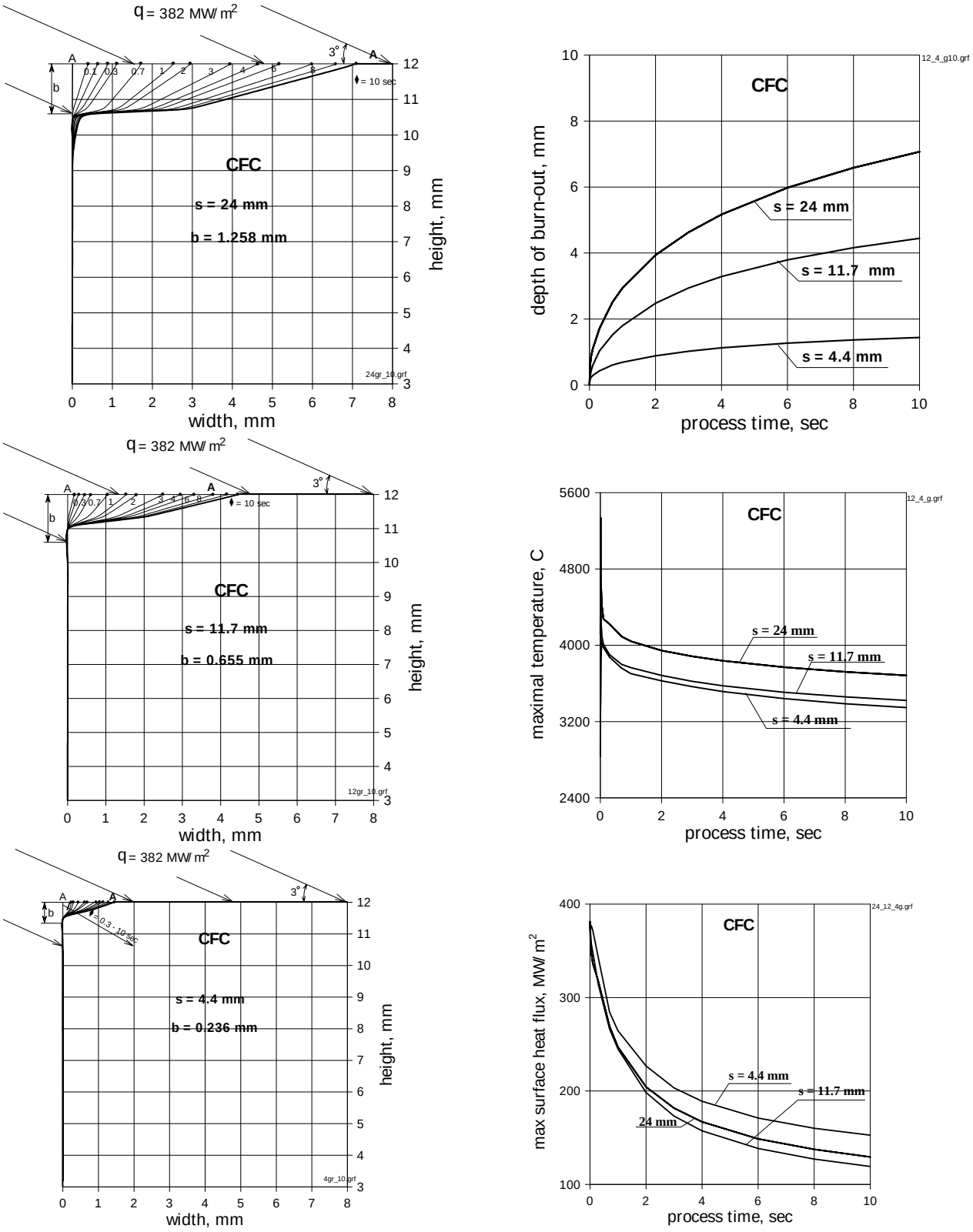

Fig. 9. Evolution of maximal temperature (A), maximal heat flux and surface profile at concentrated lateral heat load.

Material – CFC (MFC-1), tile height (h_1) = 10 mm

Tile on separate interlayer

Tile width (s) = 4.4, 11.75, 24 mm

Area of lateral heat load (b) = 0.236, 0.655, 1.258 mm

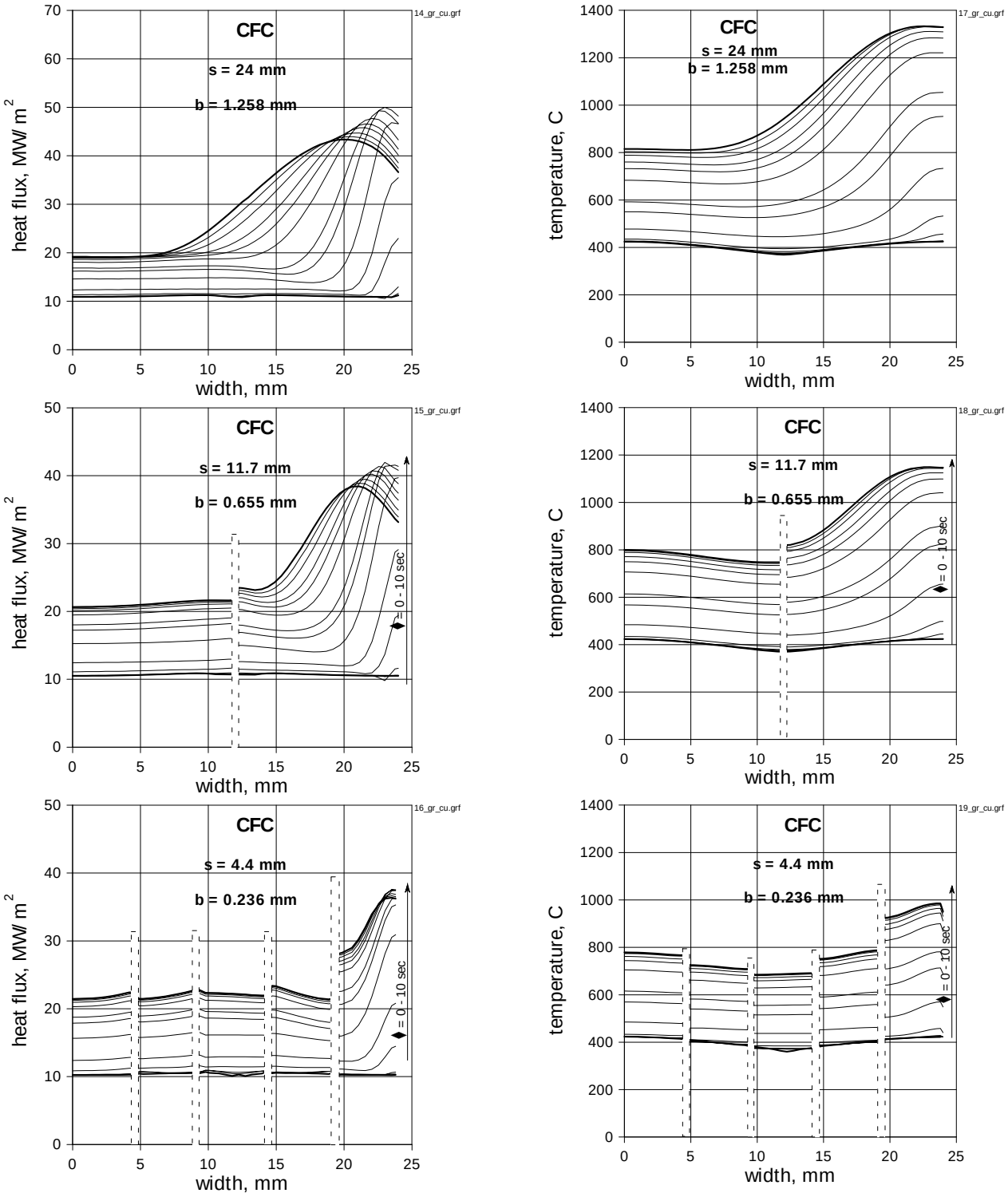

Fig. 10. Evolution of heat flux and temperature distribution in the CFC/Cu joint

Material – CFC (MFC-1), tile height (h_1) = 10 mm
Tile on separate interlayer
Tile width (s) = 4.4, 11.75, 24 mm
Area of lateral heat load (b) = 0.236, 0.655, 1.258 mm

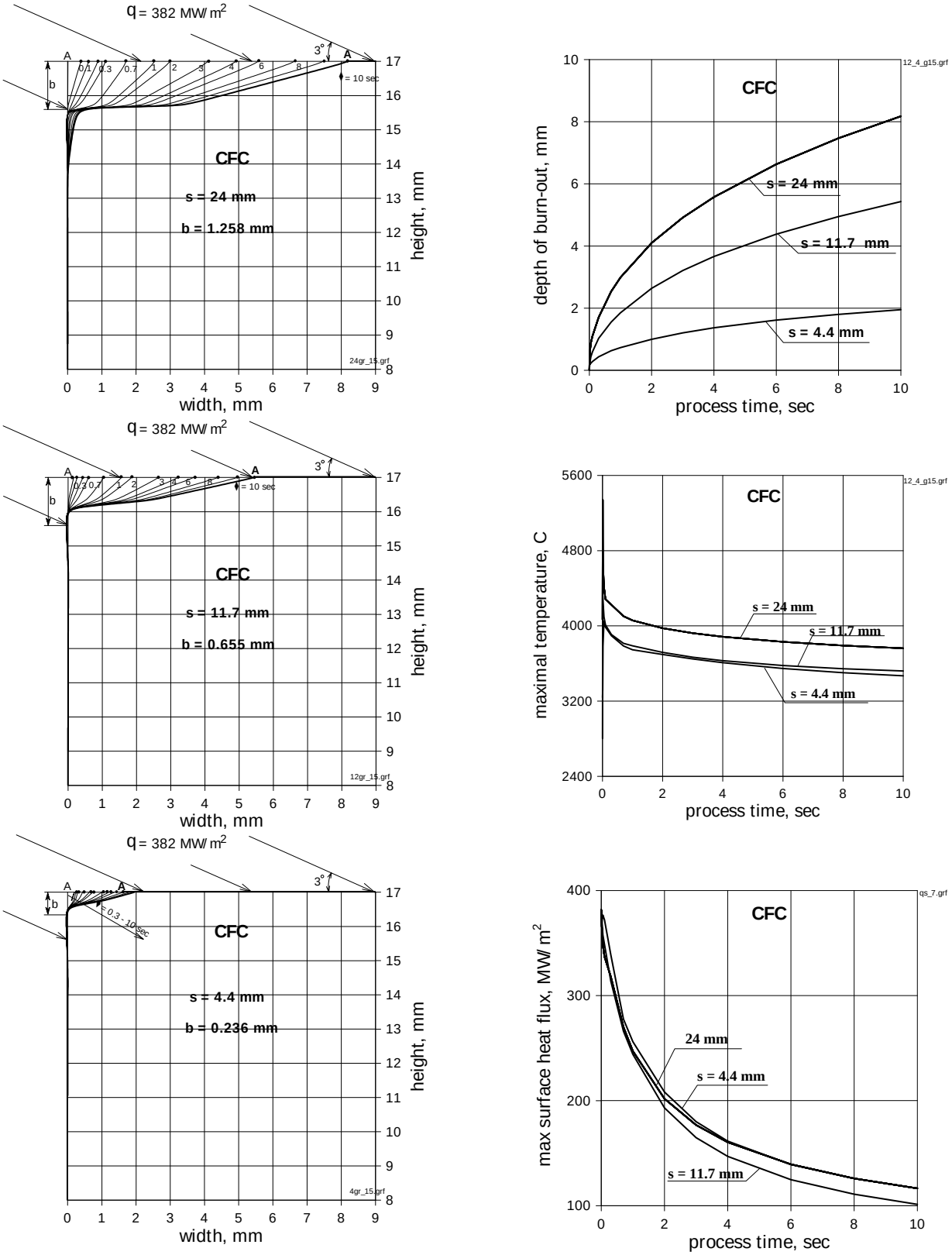

Fig. 11. Evolution of maximal temperature (A), maximal heat flux and surface profile at concentrated lateral heat load.

Material – CFC (MFC-1), tile height (h_1) = 15 mm

Tile on separate interlayer

Tile width (s) = 4.4, 11.75, 24 mm

Area of lateral heat load (b) = 0.236, 0.655, 1.258 mm

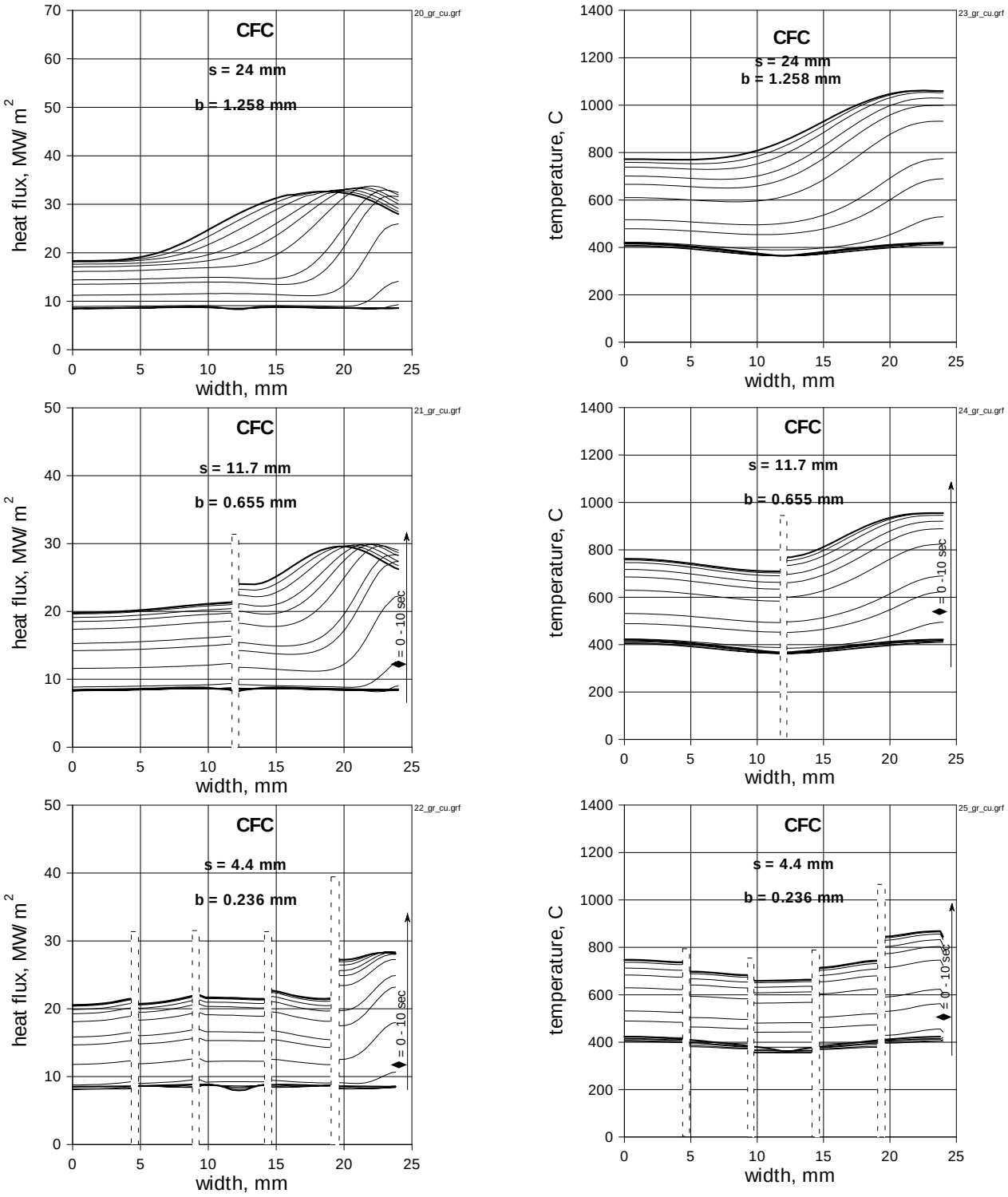

Fig. 12. Evolution of heat flux and temperature distribution in the CFC/Cu joint

Material – CFC (MFC-1), tile height (h_1) = 15 mm
Tile on separate interlayer
Tile width (s) = 4.4, 11.75, 24 mm
Area of lateral heat load (b) = 0.236, 0.655, 1.258 mm

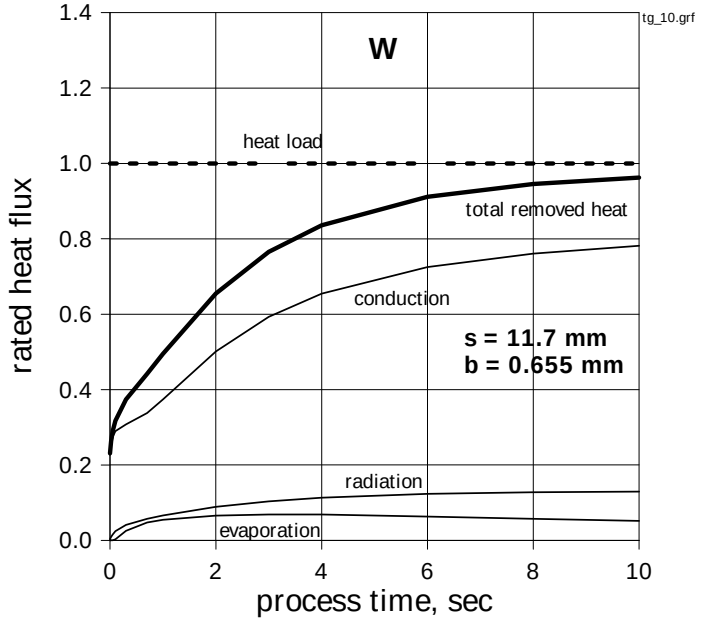

Fig. 13. Evolution of heat balance

Material – W-alloy (1% La_2O_3), tile height (h_1) = 10 mm
Tile on separate interlayer
Tile width (s) = 11.75 mm
Area of lateral heat load (b) = 0.655 mm

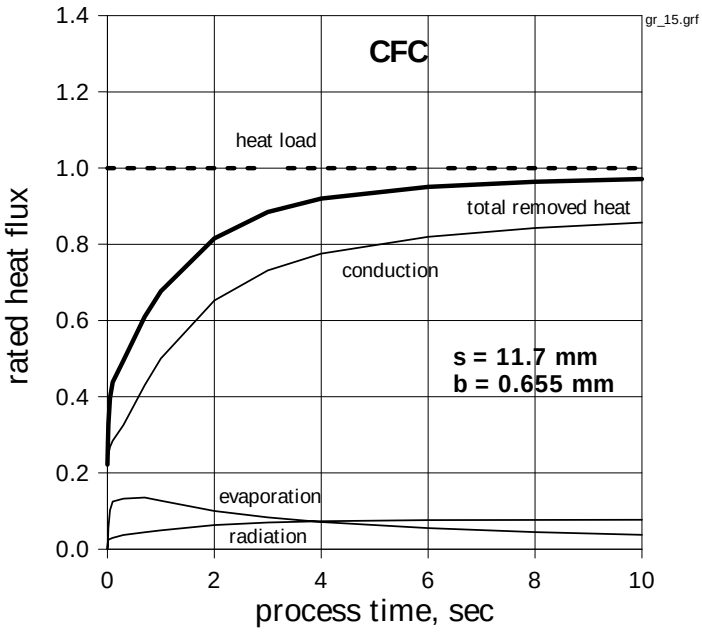

Fig. 14. Evolution of heat balance
Material – CFC (MFC-1), tile height (h_1) = 15 mm
Tile on separate interlayer
Tile width (s) = 11.75 mm
Area of lateral heat load (b) = 0.655 mm

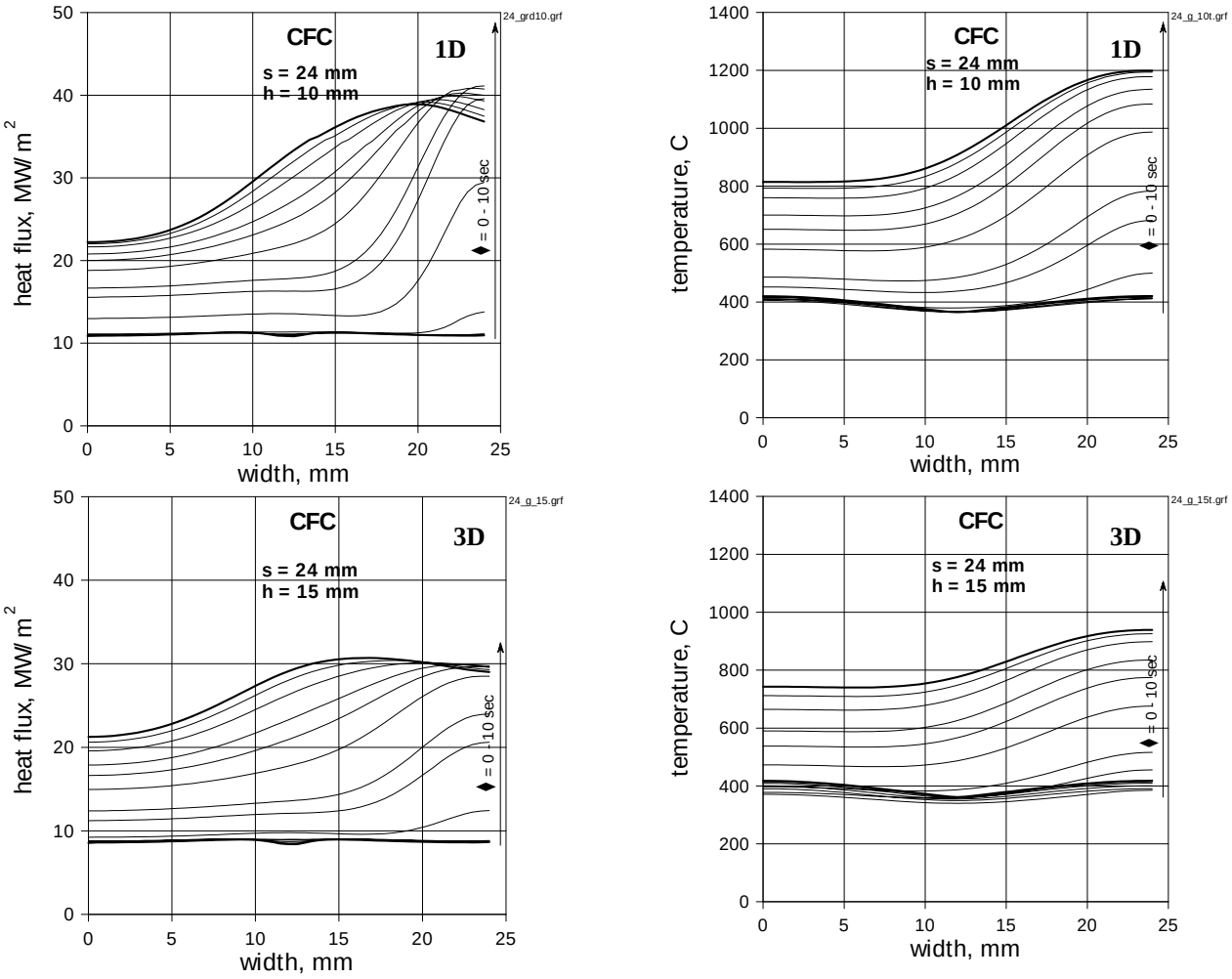

Fig. 15. Comparison of two types CFC: MFC-1 (1-D) and Dunlop (3-D)

Evolution of heat flux and temperature distribution in the CFC/Cu joint

Material – CFC (Dunlop), tile height (h_1) = 10 mm & 15 mm;

Tile on separate interlayer

Tile width (s) = 24 mm

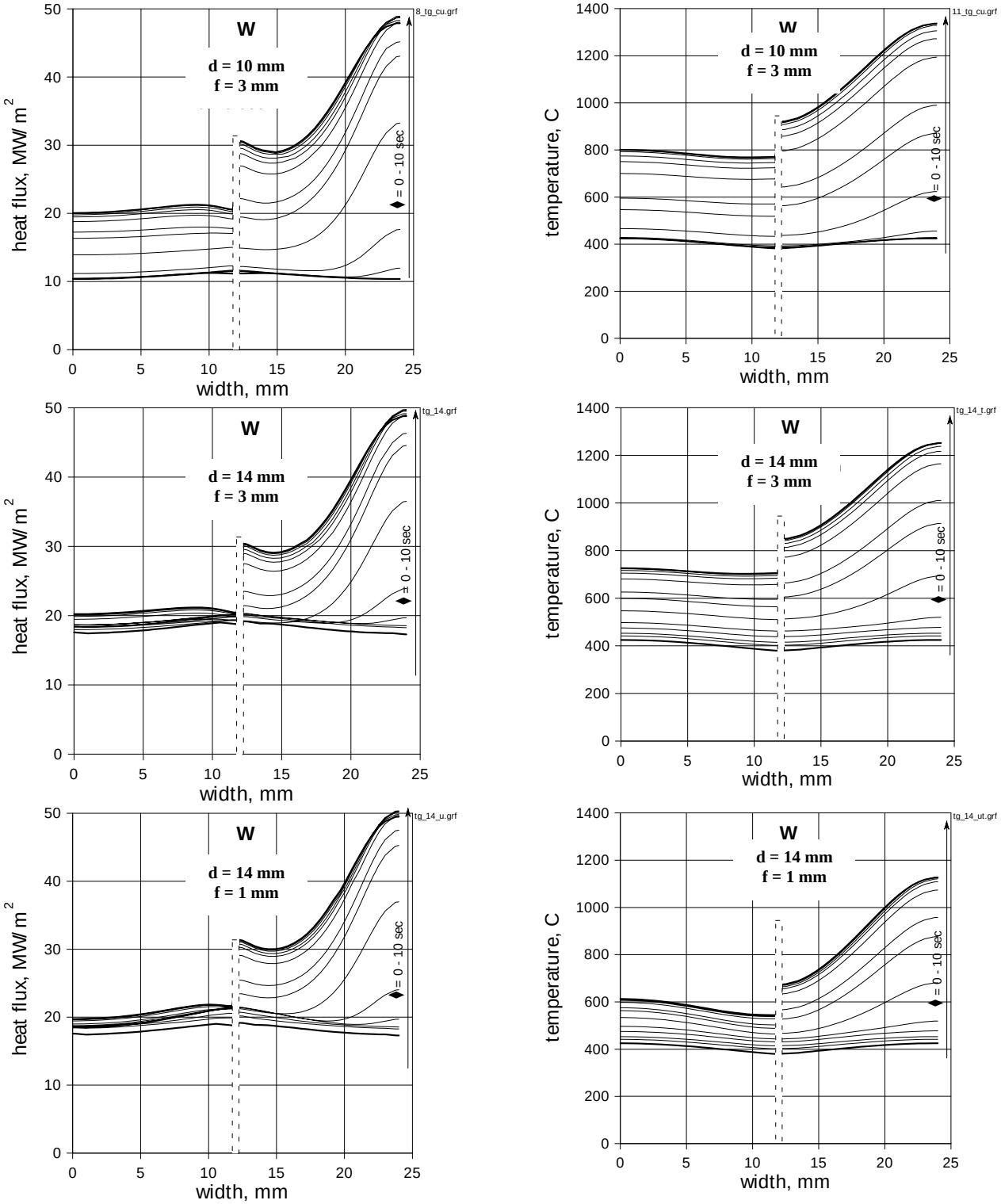

Fig.16. Influence of cooling channel diameter (d) and bronze ligament above the coolant channel (f) on heat flux and temperature distribution in the W/Cu joint

Material – W-alloy (1% La_2O_3), tile height (h_1) = 5 mm
Tile on separate interlayer
Tile width (s) = 11.7 mm

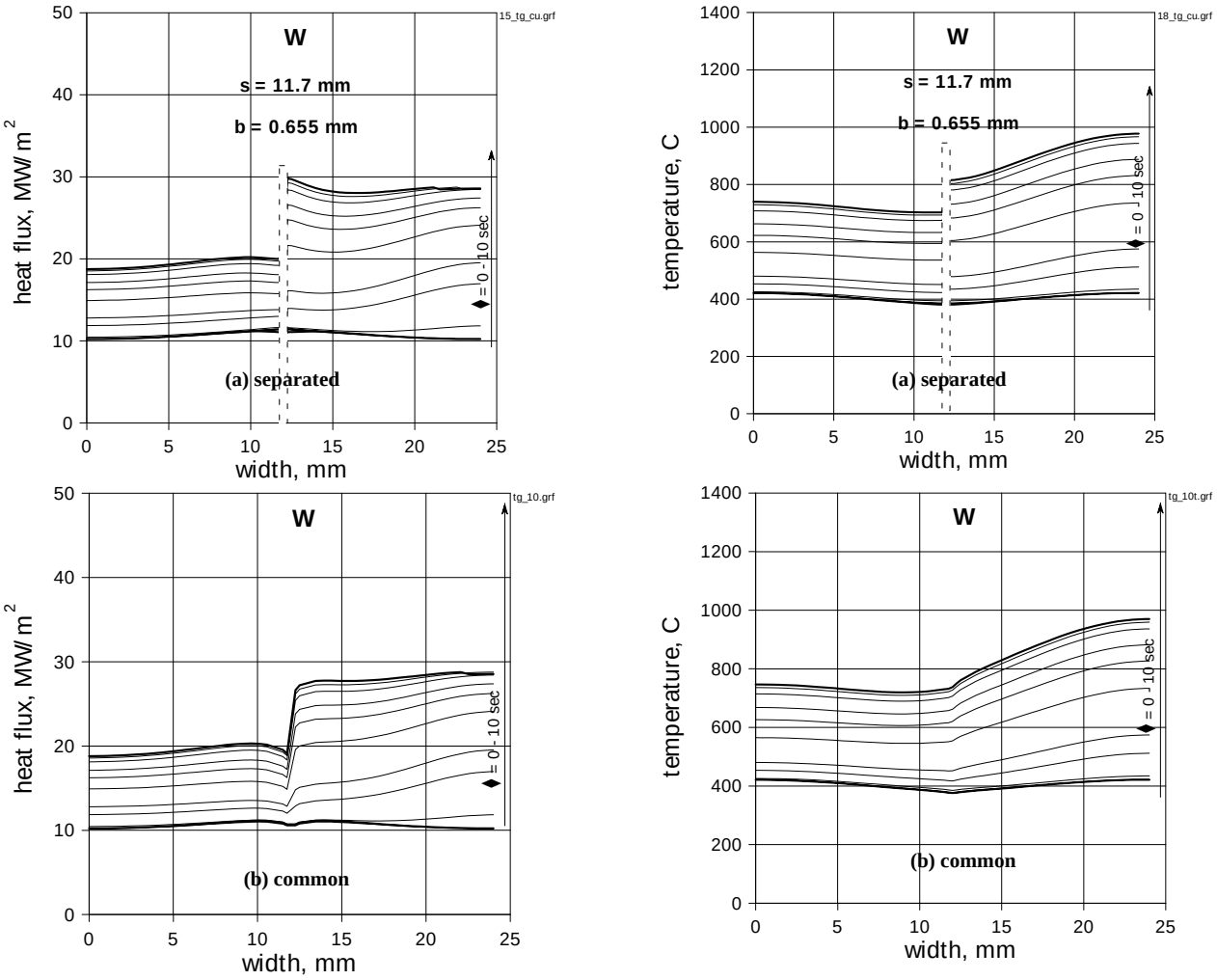

Fig.17. Comparison of two interlayer design options: (a) separated and (b) common

Material – W-alloy (1% La_2O_3), tile height (h_1) = 10 mm
Tile width (s) = 11.7 mm

Two design options of the interlayer: (a) separate interlayer for each tile and (b) common interlayer for all tiles, were under analysis. The obtained results shown in Fig. 17 reveal not significant difference in their performance, at least, for option being under consideration.

Fig. 18 shows results of computation which has been carried out as an analytical support to the experiments performed in SNLA (USA) on fatigue tests of divertor small-scale mock-ups under heat loads simulated SOL conditions. Analytical simulation of cascade effect for corresponding geometry is shown in Fig.19. It can be concluded from comparison of Fig.18 and Fig.19 that this armour design is resistant to cascade effect failure.

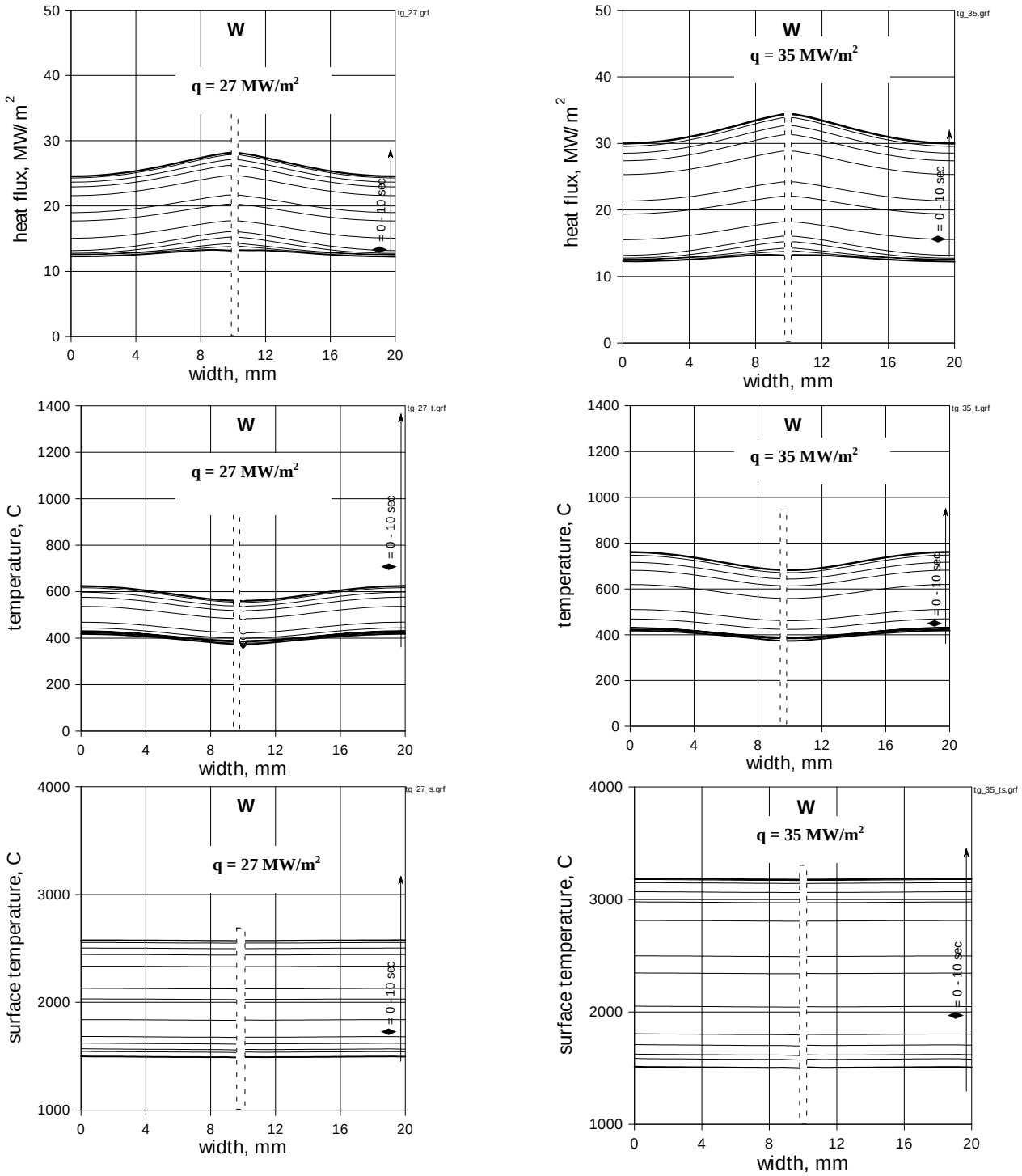

Fig. 18. Evolution of heat flux and temperature distribution in the W/Cu joint and on the tile surface

Calculation in support of mock-up tests in SNLA

Test condition: q = 27 & 35 MW/m^2

P = 1.43 MPa ; T_{water} = 17 ℃ ; W_{water} = 15 m/s

Smooth channel d = 12 mm (no enhancer)

Material – pure W, tile height (h_1) = 10 mm

Tile on separate interlayer

Tile width (s) = 9.7 mm

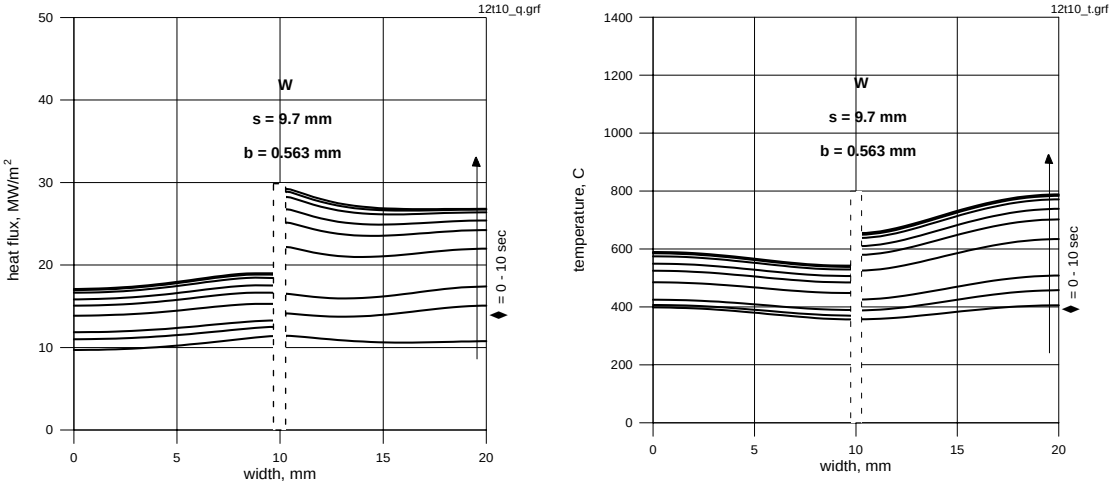

Fig. 19. Evolution of heat flux and temperature distribution in W/Cu joint

Material – W, tile height (h_1) = 10 mm

Two tiles on separate interlayer

Tile width (s) = 9.7 mm

Area of lateral heat load (b) = 0.563 mm

Channel diameter (d) = 10 mm

Copper ligament above the cooling channel is 1 mm

Water condition: 4.3 MPa, t=100 C, v=10 m/s

5. Conclusion

The presented results demonstrate the developed code high ability to perform the transient thermal analysis on 2-D models with the complex non-linear boundary conditions, which includes:

- heat lost by radiation from the element external surface;
- evaporation of material;
- evolution of the loaded surface profile due to its erosion;
- dependence of the heat transfer coefficient from the cooled wall local temperature
- flow regime comprises all heat exchange modes: from single phase forced convection to post-CHF zone.

The performed thermal analysis of the vertical target subjected to highly concentrated ($q_o \approx 382$ MW/m^2) near normal heat load caused by the loss of an upstream tile makes possible to draw the following conclusions:

1. The concentrated heat load onto the vertical target tile caused by the loss of an upstream tile results in erosion of the plasma facing surface for both tungsten and CFC armours, which creates the potential of "plasma machining" for the divertor PFC's.

2. The maximum erosion depth (in direction of SOL impact) is a similar for both tungsten and CFC armours and depends from the tile height (h_1) and width (s) as follows: the higher and wider is the tile, the higher is the erosion.

3. Plasma machining of the tile surface makes possible to reduce significantly the maximum surface heat flux (from ~ 400 MW/m^2 down to~ 100 MW/m^2) as well as the surface temperature (from ~ 6400°C down to ~ 4800°C) resulting in reduction of thermal stresses in the near surface area. Latter decreases a probability of cracks generation in this region.

4. An erosion process is close to, but does not reach its saturation within a single pulse. Apparently, 3 – 10 transient pulses are needed to stop plasma machining of PFC's.

5. About 20 % of the incident heat load is lost by material evaporation and radiation from the vertical target external surface, by this way helping to relieve slightly the interlayer and cooling channel from the heat load.

6. It is recommended to avoid the use of the vertical target with tungsten wide (s = 24 mm) and low height (h_1 = 5 mm) tiles due to the potential of the development of total heat removal crisis in the water cooling channel resulting in its complete destruction.

7. The lost of a tile and resulting the SOL intercepting by the leading edge of the downstream tile causes the heat flux and temperature distribution in the armor/heat sink joints to high non-uniformity, which creates the problem with the vertical target integrity. The use of high and narrow tiles makes possible to flattening the heat flux and temperature distribution in the armor/heat sink joints.

8. In case of short and wide tiles the interlayer temperature exceeds its melting value (see Fig. 6 and Fig. 10) over almost the half tile width. An attempt to reduce this temperature by applying the bigger channel diameter (d = 14 mm instead of d = 10 mm) or the thinner heat sink (c = 8 mm instead of c = 10 mm) (see Fig. 16) reveals, that only the heat sink decrease gives us more or less acceptable results: 200 C temperature reduction in the interlayer.

9. An application of 3-D CFC (Dunlop) is a preferable to make the heat flux and temperature distribution more uniform, but gives not much credit (see Fig. 15).

10. The similar: the design option with the separate interlayer under each tile is slightly better than the option with the common interlayer for all tiles.

References

1. *Technical basis for the ITER-FEAT outline design, Draft for TAC Review*. **GAO RI2 99-12-12 W 0.3**, December 12, 1999

2. J.G. van der Laan, M. Akiba, A. Hassanien, M. Seki, V. Tanchuk *Prediction for disruption erosion of ITER PFC.* ISFNT-2, Karlsruhe, June 2 – 7, 1991

3. V. Divavin, V. Tanchuk, L. Ogej *Cooling system and temperature state of the divertor target.* **ITER IL-PC-8-0-3**, January, 1990.

4. S. Grigoriev, V. Tanchuk *Thermophysical analysis of the ITER divertor targets. USSR Contribution on PFC.* **ITER IL-PC-1-0-9**, July, 1990.

5. V. Divavin, A. Mikhailov. *Temperature response of the tokamak First Wall on heat loads produced by plasma distribution*. Journal of Technical **Physics V. 54, N 3**, 1984 (in Russian).

6. G. Mueller, D. Strauss, F. Zimmermann, V. Engelko, A.Andreev *Conceptual Design of the Pulsed Electron Beam Facility GESA II.*

7. V. Divavin, V. Tanchuk, A. Shrubok, R. Watson, J. Gonsalez *An experimental and numerical investigation of post-CHF heat transfer for one-sided heat load with highly subcooled flow boiling*. Fusion Engineering and Design Journal, Submitted November, 1993.

8. *Design Task of Neutral Beam Injector – Final Report of Efremov Design Office*. June 30, 1998.

9. A. Uglov, O. Sagdedinov. *On evaluation of metal melting by a volumetric heat source.* Journal of Engineering Physics, **V.65, N 5**, pp. 594 – 597, May 1993 (in Russian).

10. A. Uglov, O. Sagdedinov. *On calculation of metal melting and solidification under the pulsed impact of concentrated energy flux*. Physics and Chemistry of Material Treatment, **N 5**, 1991, pp. 36-40 (in Russian).

11. A. Uglov, U. Smurov, A. Lapshin. *Simulation of non-steady-state phase boundary motion under high power impact on materials.* Thermal Physics of high temperature. **V.27, N1**, pp. 87-93, 1989.

12. A. Markov, V. Rotshtain. *Calculation and experimental determination of depth of strengthening and tempering zones in hardened steel U7A, exposed to the pulsed e-beam.* Surface, **N 4**, pp. 83 – 89, 1998

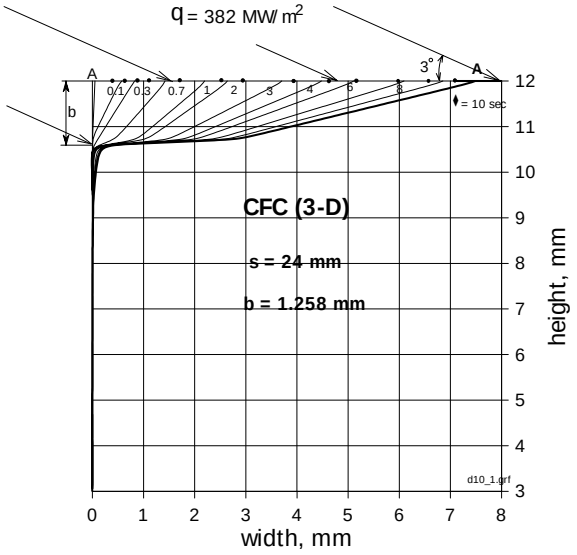

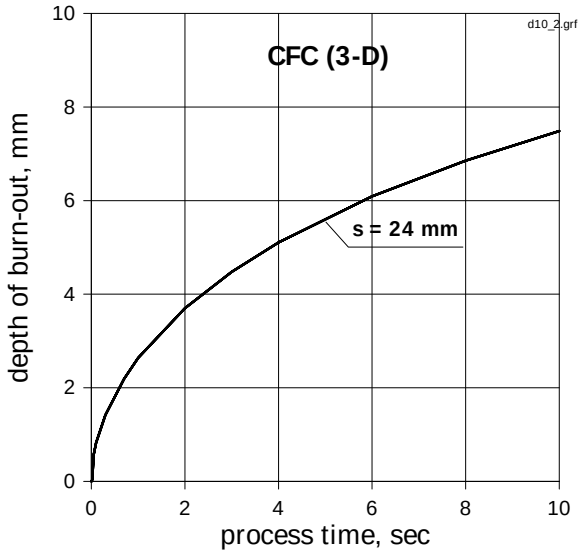

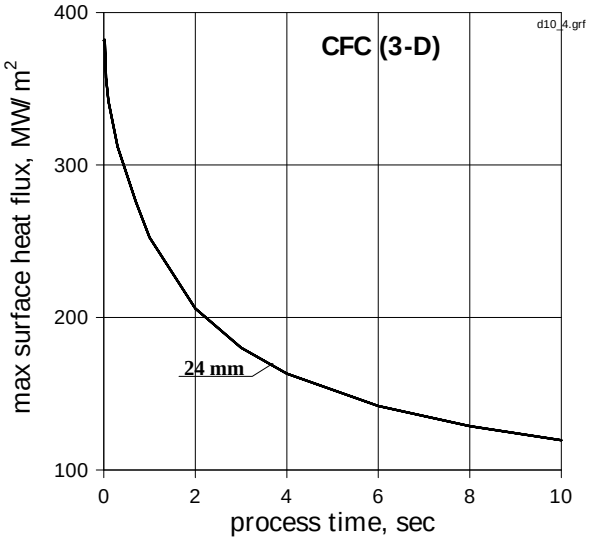

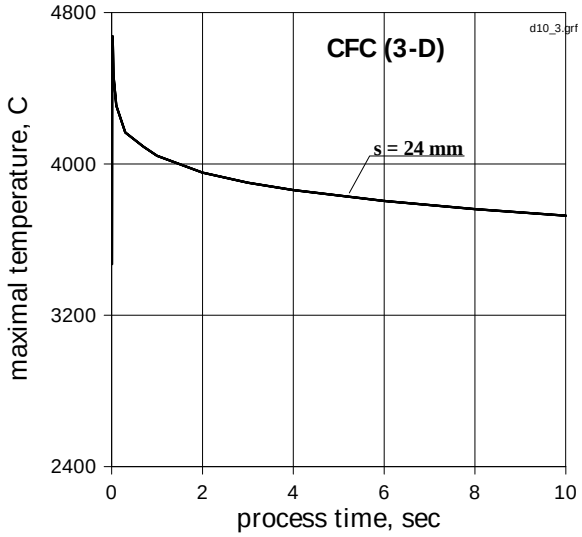

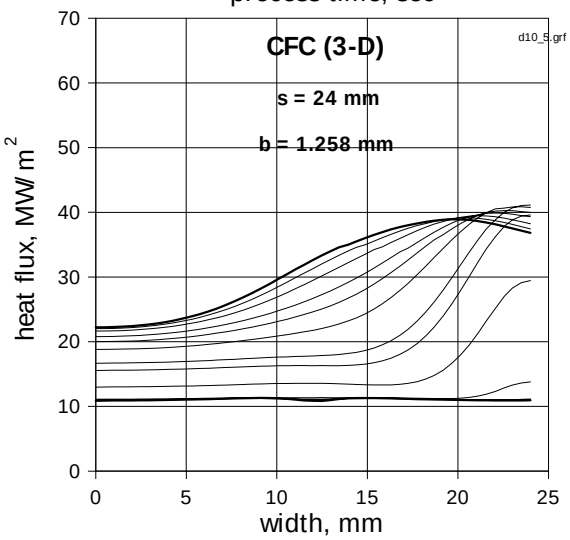

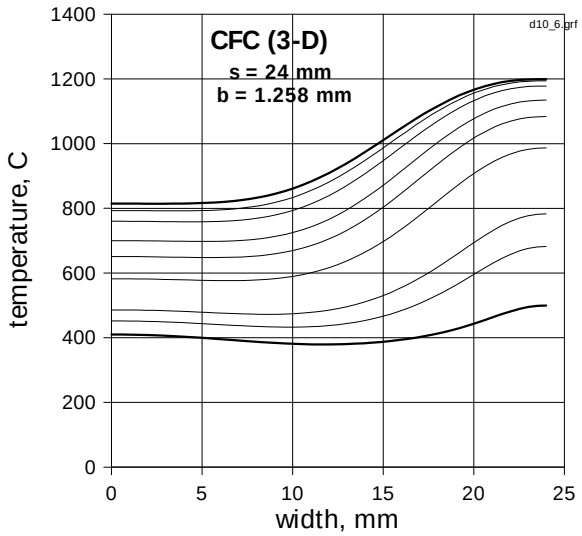

Material – CFC Dunlop (3-D), tile height (h_1) = 10 mm

Tile width (s) = 24 mm

Area of lateral heat load (b) = 1.258 mm

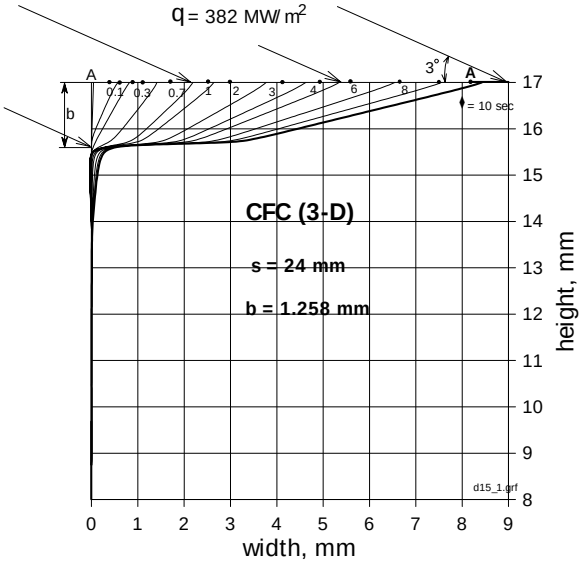

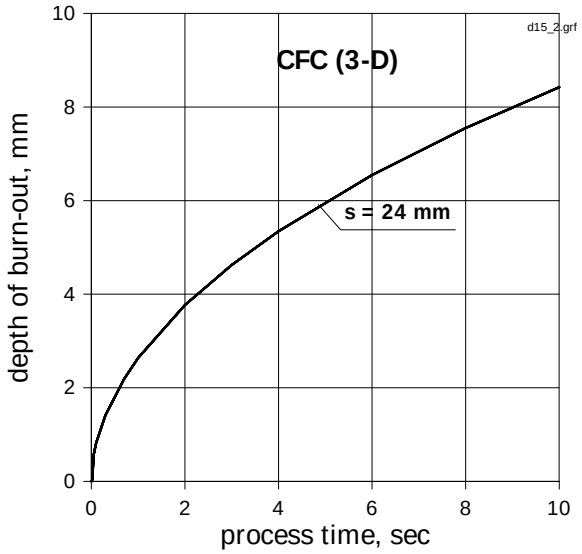

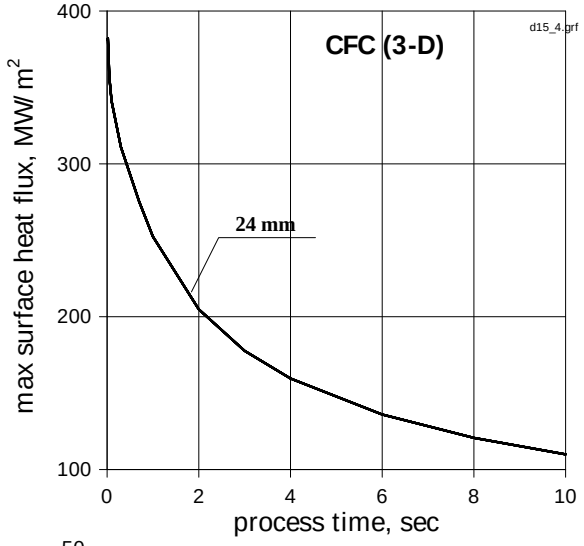

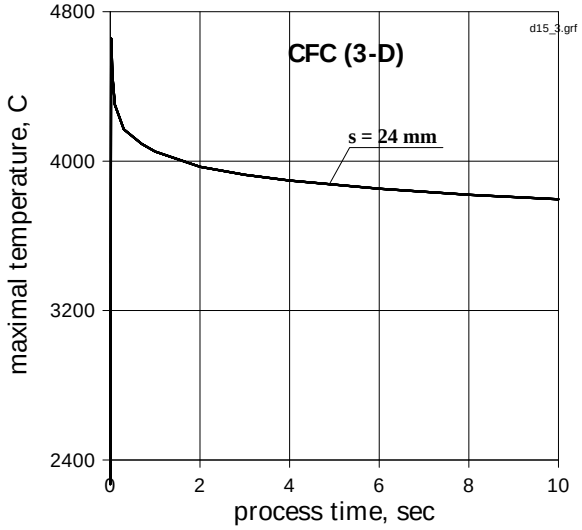

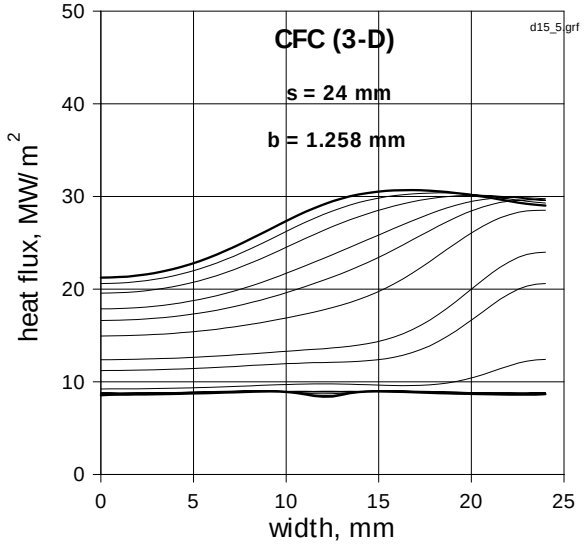

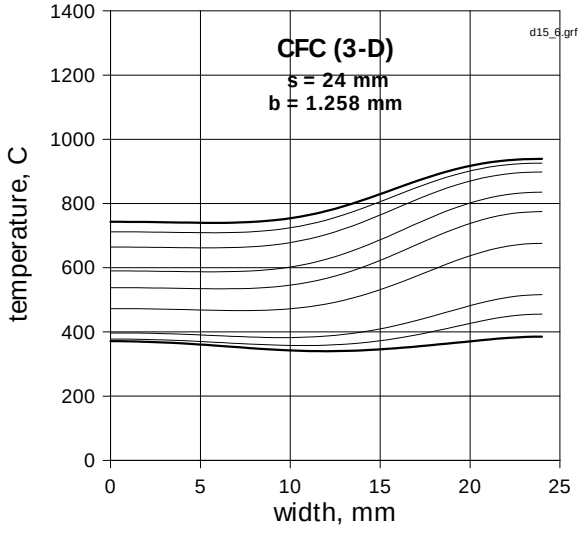

Material – CFC Dunlop (3-D), tile height (h_1) = 15 mm

Tile width (s) = 24 mm

Area of lateral heat load (b) = 1.258 mm